Metamaterial design for middle-low frequency elastic wave mitigation

H.Y.Y. Shi, T.E. Tay and H.P. Lee

Department of Mechanical Engineering, National University of Singapore, Singapore

ABSTRACT

In the past two decades, meta-materials have drawn increasing attention from researchers due to their unique properties, including wave attenuation with potential application in acoustic engineering. A number of meta-material designs have been proposed for wave attenuation at different frequencies. In this work, a new configuration of chiral honeycomb meta-material is proposed for the attenuation of middle-low frequency elastic waves. The dynamic characteristics of the new-proposed structure were investigated numerically with band diagram analysis. The results show that the proposed structure is able to create multiple band gaps at middle frequency range. Interestingly, two extra band gaps induced by local resonance effect can be created with reduction of the chiral angle of the unit cell, and one of the bandgaps is located at low frequency range. The wave attenuation performance of the proposed meta-material was also simulated using sound transmission loss finite element analysis, demonstrating the potential of the structure in real applications.

1 INTRODUCTION

Meta-materials have become a popular research topic due to their unique properties including auxetic behavior (also known as negative Poisson's ratio) (Lakes *et al.*, 1987, Evans *et al.*, 1991, Prall, D. *et al.*, 1997), negative effective elastic constants and ability for wave attenuation (Liu, Z. *et al.*, 2000), as well as wave guide and mitigation properties of periodic lattice structures (Brillouin, Leon, 1946, Mead, D. M, 1996, Phani, A. S. *et al.*, 2006). These properties can be altered by manipulating spatial arrangement of the cellular structure, which provides flexibility in design and function optimization.

Potential wave attenuation by meta-materials design is particularly attractive for application in optical and acoustic engineering. The characteristics of phononic structures have been examined by physicists and engineers, and the study has been extended from optical to acoustic waves. Much work has been done to determine the relationship between lattice geometry and characteristic bandgaps (Phani, A. S. *et al.*, 2006, Wu, Fugen *et al.*, 2002). In some studies, phononic crystal structure was modelled as equivalent mass-spring systems (Jensen, J. S., 2003, Aly, A. H. *et al.*, 2012). Ruzzene *et al.* (2003) claimed in his work that the re-entrant geometries with negative Poisson's ratio were effective in constraining wave propagation directionally. Most of the phononic structure exhibits wave attenuation properties in the stop band frequency due to the Bragg scattering phenomenon, however, this phenomenon limits the frequency range of waves that can be attenuated given the dimensional constraint of some phononic structures. To handle low frequency elastic waves, Liu, Z. *et al.* (2000) proposed the concept of locally resonant structure and the analytical solutions were provided in his later work (Liu, Z. *et al.*, 2005). Thereafter, more research has been done on locally resonant materials, including investigation of the influence of negative elastic constants on low frequency wave propagation (Huang, H. H. *et al.*, 2011, Huang, G. L. *et al.*, 2009, Tan, K. T. *et al.*, 2014, Ding, Y. *et al.*, 2007, Wang, P. *et al.*, 2014). Additionally, the membrane type metamaterial with negative effective density was also proposed for the consideration of weight reduction (Yang, Z. *et al.*, 2008, Park, C. M. *et al.*, 2011, *Sui, N.* et al., 2015).

In order to widen the range elastic wave filtering properties of meta-materials, Liu, X. N. *et al.*, 2011, and Zhu, R. *et al.*, 2014 proposed integrating the concept of "coating ball" into the hexagonal chiral honeycomb structure. The literature attributes the formation of low-frequency band gap to the local resonance effect of coating ball, and the higher band gap to the Bragg scattering effect induced by the base structure. Previous to these works, Spadoni *et al.* (2009) had done a comprehensive study on the phononic properties of hexagonal chiral lattices. His work suggests that the pure hexagonal structure is able to create multiple band gaps at high-frequency range, which are induced by the bending deformation of the ligaments, and therefore strongly affected by structural stiffness.

The main focus of this study is on the planar (2D) meta-material design for in-plane wave filtering at the middle-low frequency range (1Hz~2300Hz). Hexagonal chiral honeycomb structure was adopted as the basic building block. However, instead of placing the coating mass into holes of the base structure, we propose a simpler composite meta-material structure by directly inserting mass inclusion into the main structure. In addition, soft

material was proposed for the hexagonal chiral honeycomb structure to lower the bandgap associated with the base structure to relatively low frequency range. The dynamic characteristics of the proposed unit cell were analyzed numerically, and the band diagram of the proposed structure was compared with that of the pure chiral honeycomb structure without mass inclusion. After that, the influence of chiral angle variation on the bandgaps was analyzed. A modified structure was then proposed as the internal structure of a sandwich panel. At last, with finite element analysis techniques, a 2D acoustic test was conducted numerically to investigate the sound insulation performance of the sandwich panel.

2   GEOMETRIC CHARACTERISTICS AND COMPUTATIONAL METHODS

Hexagonal chiral honeycomb was adopted as the main structure. The structural layout of a basic hexagonal chiral lattice is shown in Fig 1. This structure consists of circular nodes with outer radius of R, and inner radius r. Circular nodes are arranged to form a hexagonal lattice structure. They are connected to each other by ligaments, and the distance between adjacent nodes is L, which is also defined as the lattice constant. The thickness of ligament is t. Chiral angle a is the angle between virtual line connecting two adjacent nodes and the corresponding ligament. Various combinations of these five parameters offer flexible choices for structural designs.
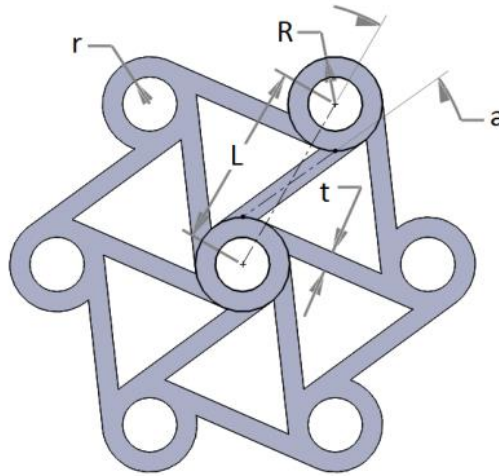

Figure 1: Geometry of chiral honeycomb structure

The proposed lattice structure and unit cell are presented in Fig 2 (a). The location of a basis unit cell is represented as $\vec{x_0}$, the lattice vectors can be expressed by lattice constant L and an orthogonal unit vector basis $\vec{l_1}$ and $\vec{l_2}$ as

$$\vec{e_1} = \frac{\sqrt{3}}{2}L\vec{l_1} + \frac{1}{2}L\vec{l_2} \tag{1}$$

$$\vec{e_2} = -\frac{\sqrt{3}}{2}L\vec{l_1} + \frac{1}{2}L\vec{l_2} \tag{2}$$

Therefore, the location of any unit cell within the entire lattice structure can be expressed by using lattice vectors and the location of reference unit cell as

$$\vec{x} = \vec{x_0} + n_1\vec{e_1} + n_2\vec{e_2} \tag{3}$$

In order to investigate the characteristics of elastic wave propagating in the periodic lattice structure, the Bloch theorem is employed (Brillouin, Leon., 1946) and the wave function can be expressed as

$$U_{\vec{x}} = Ae^{i(\omega t - (\vec{k}\cdot\vec{x}))} \tag{4}$$

where A is the wave amplitude, ω is the wave frequency and $\vec{k}$ is the wave vector. The wave function at any location within the lattice structure can be represented by

$$U_{\vec{x}} = U_{\vec{x_0}}e^{i\vec{k}\cdot(\vec{x}-\vec{x_0})} \tag{5}$$

This relation describes the periodic boundary condition of the unit lattice. It should be noted that the wave vector $\vec{k}$ can be expressed as

$$\vec{k} = \alpha_1 \vec{b_1} + \alpha_2 \vec{b_2} \qquad (6)$$

with $\vec{b_1}$ and $\vec{b_2}$ being reciprocal lattice vectors, defined as

$$\vec{b_i} \cdot \vec{e_j} = 2\pi \cdot \delta_{ij} \qquad (7)$$

Where δ_{ij} is Kronecker delta and is defined as

$$\delta_{ij} = \begin{cases} 0 \text{ if } (i \neq j) \\ 1 \text{ if } (i = j) \end{cases} \qquad (8)$$

Therefore from equation (1), (2), (7) and (8), the magnitude of reciprocal lattice vectors $\left|\vec{b_i}\right|$ can be calculated to be $\frac{4\sqrt{3}\pi}{3} R$, and the First Brillouin Zone and Irreducible Brillouin zone (IBZ) can be constructed in Fig 2 (b). The IBZ, defined by boundaries OA, AB and BO, is the smallest space required to determine the maximum frequency range of the wave which is allowed to pass through this particular lattice structure.
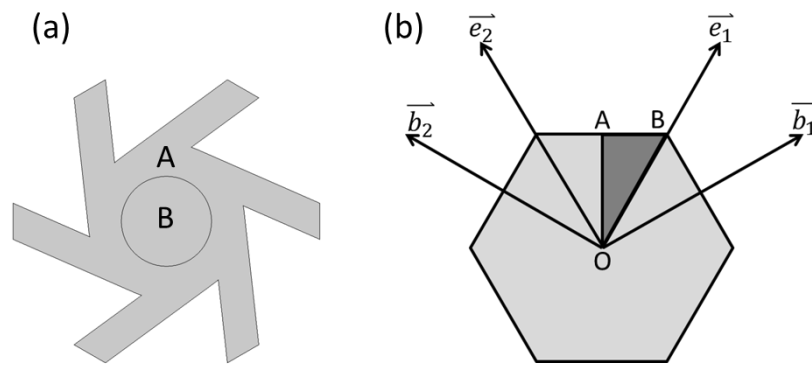

Figure 2: (a) Proposed structure unit cell (b) The first Brillouin Zone of the unit cell

In order to investigate the dynamical characteristics of the proposed lattice structure, finite element analysis technique was used. A numerical model was constructed. The soft material TangoBlackPlus was used as the main structure and tungsten was chosen as the inclusion mass. For convenience, elastic behavior of the material was assumed. Therefore the soft elastic material ($\rho = 1.13 \times 10^3 \text{kg/m}^3$, $E = 0.48$ MPa, $\upsilon = 0.49$) was applied to the hexagonal chiral honeycomb structure A, and the tungsten properties ($\rho = 19 \times 10^3 \text{kg/m}^3$, $E = 411$ GPa, $\upsilon = 0.3$) was used for the mass inclusion B. In addition, the Bloch periodicity conditions were applied at the boundaries of the unit cell. The eigenfrequency problem of the proposed structure could be calculated using commercial software Comsol. Then the band diagram could be constructed, and the results were shown in the following section.

3 CASE STUDY RESULTS
In this section, the in-plane dynamic characteristics of the proposed chiral honeycomb composites unit cell were studied. This specific composites structure was taken as a reference configuration, and was used for comparison in the following case studies. Table 1 summarizes the geometrical parameters and mechanical properties of the reference configuration. The first case study was to compare reference configuration with pure hexagonal chiral honeycomb structure. The second case study was to compare the reference configuration with the honeycomb structure with chiral angle of 0 degree.

Table 1: Geometrical parameters and mechanical properties of reference configuration

Geometrical parameters	Value	Mechanical properties	Value
Circular node inner radius, r(mm)	1.36	Young's modulus of honeycomb structure, E_s(MPa)	0.48
Circular node outer radius, R(mm)	2.36	Poisson's ratio of honeycomb structure v_s	0.49
Distance between two nearest nodes, L(mm)	9.25	Density of honeycomb structure, ρ_s(kg/m³)	1130
Thickness of ligament, t(mm)	1.00	Young's modulus of mass inclusion, E_m(GPa)	411
Chiral angle, a(degree)	23.72	Poisson ratio of mass inclusion, v_m	0.3
		Density of mass inclusion, ρ_m(kg/m³)	19000

3.1 Band diagram

Band diagram is a convenient representation of the dispersion characteristics of the analyzed structure. In the band diagram, the frequency of propagating wave in the structure is plotted against the wave vector as it varies along the contours of the irreducible Brillouin Zone (IBZ), which can be represented by the outline O-> A-> B-> O shown in Figure 2 (b). Each band (curve) represents the dispersion curve for each wave mode. By varying the wave vector along IBZ, the frequency range of each wave mode can be determined, and therefore the locations and ranges of bandgaps can also be determined. The band diagram was constructed based on information provided in Section 2. To justify the function of mass inclusion in our composite structure, the comparison has been made between the band diagrams of the reference configuration and pure hexagonal chiral honeycomb. The results are shown in Fig. 3.
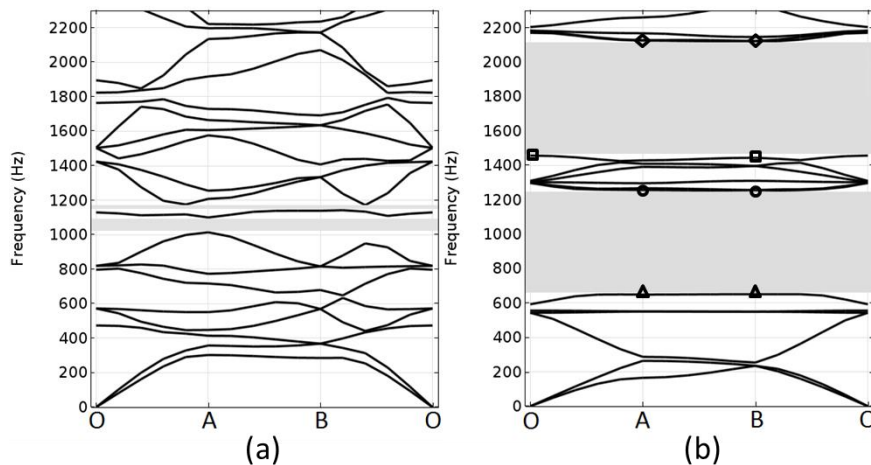

Figure 3: Band diagram of (a) pure hexagonal chiral honeycomb structure (b) the proposed composite structure (reference configuration)

The results show that before the mass inclusion was inserted, the hexagonal chiral honeycomb was able to create two bandgaps located between 1000Hz to 1200Hz, but these two bandgaps are extremely narrow and so of very limited effect on wave filtering. However, after the insertion of the mass inclusion, the mass not only changes the boundary condition of the ligaments, but also restricts the deformation of the circular nodes. Therefore the bands experience large changes in terms of shape and location, and these changes lead to the disappearance of the narrow bandgaps in Figure 3 (a) and the creation of two new bandgaps in Figure 3 (b). At this stage, with this typical geometry configuration and material selections, it is intuitive to relate these two bandgaps with the "mass-in-mass locally resonant system" (Liu, Z. *et al.*, 2000, Liu, X. N. *et al.*, 2011).
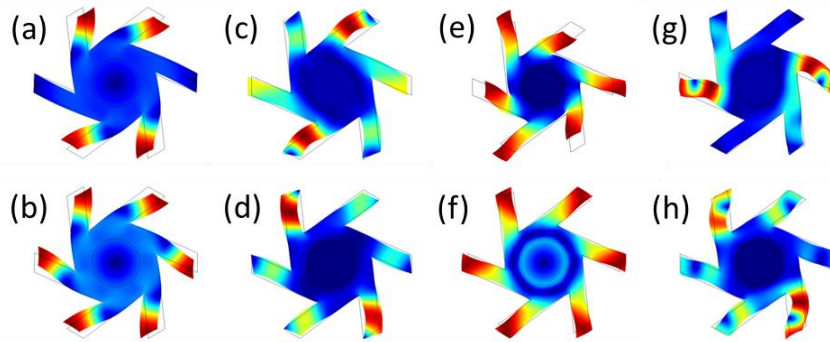
3.2 Vibration mode

Figure 4: Mode shapes for proposed composite structure: (a-b) bottom edge of first bandgap; (c-d) top edge of first bandgap; (e-f) bottom edge of second bandgap; (g-h) top edge of the second bandgap.

It is necessary to analyze the associated vibration modes in order to understand the formation of the bandgaps. Fig. 4 shows the vibration modes of the proposed composite structure on the dispersion curves located at the edges of bandgaps, with (a), (c), (g) showing the modes at A of Fig.3; (e) at O of Fig.3; and (b), (d), (f), (h) at B of Fig.3. The locations O, A and B are indicated in Fig. 3. It is observed that these vibration shapes, mainly of the ligaments, are complex mixed modes, while the inclusion mass remains largely stationary in all cases. This shows the fundamental difference between the proposed composite structure and the coating ball composite structure proposed in Liu *et al.*'s (2011) and Zhu, R *et al.*'s (2014) work. In their work, there is always strong coupling between the resonance of mass inclusion and the propagation elastic wave in the formation of bandgaps. Within those bandgaps, the mass inclusion functions as a local resonator, and its direction of vibration depends on the wave mode and the wave propagation direction. However, for the meta-composite structure proposed in this work, since the mass inclusion remains stationary within all of its bandgaps, no resonance of the mass inclusion is involved in the formation of any of its bandgaps.

3.3 Chiral angle case study

The reference configuration is defined by many parameters, and those parameters can influence the formation of bandgaps. In this case study, the main focus is on chiral angle a. The reference configuration was compared with the honeycomb composites with chiral angle of 0 degree. Their unit cells are shown in Fig. 5. (a) and (b).
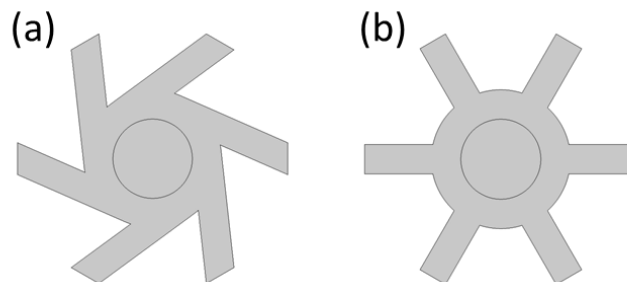

Figure 5: (a) reference configuration (b) honeycomb composites with chiral angle of 0 degree

Fig. 6 (a) and (b) show the band diagrams of these two configurations. Obviously, this variation of chiral angle *a* causes the formation of bandgap 1 in Fig. 6. (b).This chiral angle change also splits bandgap 2 in Fig. 6. (a) into bandgap 3 and 4 in Fig. 6. (b). However, the total width of the bandgap3 and the bandgap4 in Fig. 6 (b) is smaller than the bandgap 2 in Fig. 6 (a).The vibration modes shown in Fig. 6 (c) and (d) have been highlighted using a circle mark and a triangle mark in Fig 6. (b). These two modes are located at bottom-edge bands of bandgap 4 and bandgap1, and they are responsible for the formation of these two new bandgaps.
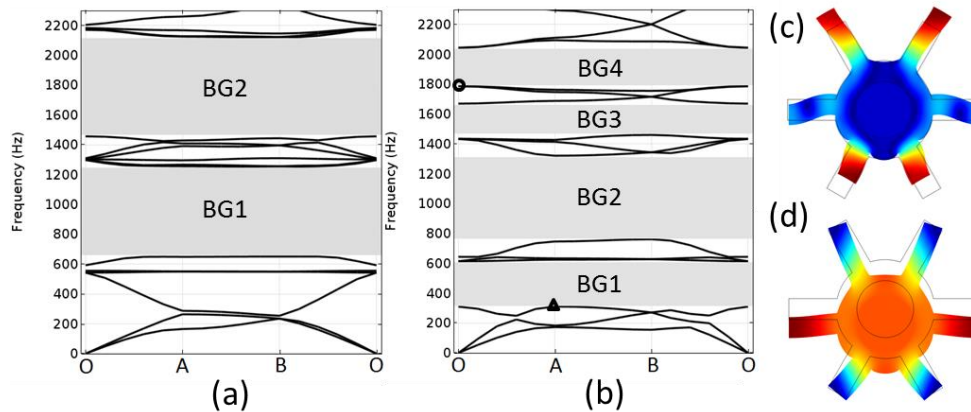
Figure 6: (a) Band diagram of reference configuration (b) Band diagram of honeycomb composites with chiral angle of 0 (c) Vibration mode of unit cell at bottom edge of BG4 (d) Vibration mode of unit cell at bottom edge of BG1

Similar bandgap-associated vibration modes have been observed by Liu, Z. *et al.* (2000). It is clear that the lower band is dominated by the oscillation of the mass inclusion, and the higher band is governed by the longitudinal vibration of the ligaments surrounding the mass, which is also known as the "optical mode". It occurs in a mass spring system with two different masses in one unit cell, and the smaller masses have much larger displacements than those neighboring larger masses. Therefore it is reasonable to conclude that the bandgap 1 and bandgap 4 in Fig. 6 (b) are induced by the local resonance mechanism. In addition, it should be noted that these two extra bandgaps do not exist in reference configuration, and the vibration modes shown in Fig. 6 (c) and (d) cannot be found in any of its bands. The large chiral angle in the reference configuration produces asymmetric forces due to the surrounding ligaments, which in turn introduce moments to the circular nodes. The translation and rotation motion of the circular nodes are coupled. Similar explanation applies to the bandgap caused by local resonance of ligaments.

4   SOUND TRANSMISSION LOSS OF 2D SANDWICH PANEL WITH PROPOSED STRUCTURE

To demonstrate the feasibility of the proposed structure in engineering application, the proposed structure is built into a sound insulation panel. A finite element analysis was used to calculate the sound transmission loss (STL) of the acoustic wave passing through the panel.

A modified lattice unit cell was used in this case. Compared with the reference configuration, the chiral angle changed to 8.59 degrees, while the rest of geometry and material properties remained the same. The lattice structure was integrated with two surface sheets to form a 2D sandwich panel to increase the bending stiffness of the panel. The STL test was conducted for the sandwich structure using commercial software Abaqus steady state dynamic analysis. A sample of 2D numerical model is shown in Fig. 7. Polylactic Acid (PLA) material properties ($\rho = 1.25 \times 10^3 \mathrm{kg/m^3}$, $E = 3.5 \times 10^9 \mathrm{Pa}$, $v = 0.3$) were applied to the surface sheets in this model. The length of the model is 100mm, and the total thickness of the sandwich panel is 51mm, including two surface sheets with 1mm thickness for each. Several layers of lattice cells were arranged in order to assure the periodicity of the structure in the direction of wave propagation, as well as eliminating obvious boundary effect. A similar numerical study methodology proposed in literature (Griese, David *et al.*, 2015), was referred in this study. For convenience, only the normal incidence wave was considered. Plane acoustic wave of unit magnitude and spectrum range from 1Hz to 2300Hz was generated below the sandwich panel, and the wave propagated upward perpendicularly to the bottom of the panel. Acoustic elements were applied at the top of the sandwich panel to monitor the acoustic pressure after the wave transmitted through the sandwich panel and thus the STL of the sandwich panel could be determined. In addition, the acoustic elements and the top layer elements of the top surface sheet were tied together. The sandwich panel was clamped in the way that both ends of each surface sheet were fixed. After the computation, the acoustic pressure P of the acoustic elements adjacent to the top surface of the panel was recorded for all the frequencies within the target spectrum, and the STL of the sandwich panel could be calculated using the following equation (Griese, David *et al.,* 2015)

$$STL(dB) = 10\log_{10}\left|\frac{\bar{p}_i^2}{\bar{p}_t^2}\right| \tag{9}$$

where $\bar{p}_i$ and $\bar{p}_t$ represent the root mean square value of the sound pressure at the incident side and transmitted side of the panel.
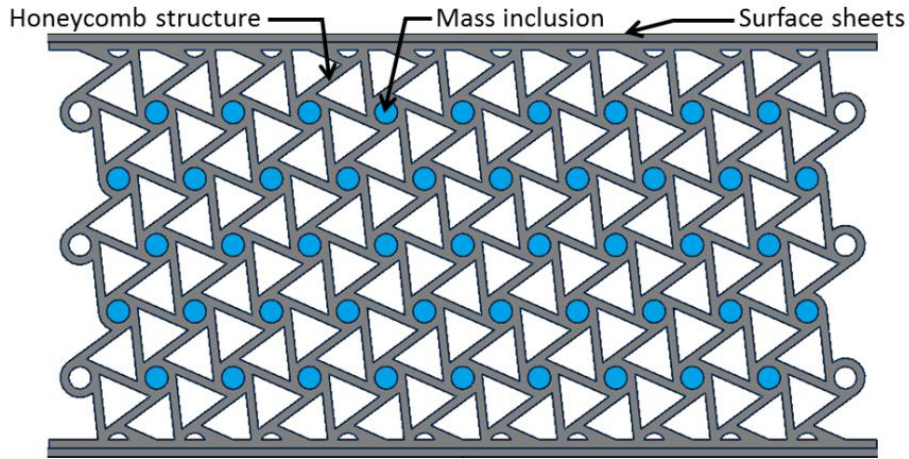

Figure 7: The Integrated sandwich panel with proposed lattice structure

Fig. 8 presents the STL test results for both cases of sandwich panels with reference configuration and modified configuration. Their corresponding band diagrams are presented aside for comparison. It is obvious that the STL test results match quite well with the band diagrams, and the correlation between the locations of STL peaks and bandgaps is obvious. All the bandgaps presented in band diagrams can be fully captured in the STL curve. This result also illustrates that locations and widths of STL peaks are controlled by the meta-material structure of the sandwich panels, demonstrating the wave filtering capability of this chiral honeycomb composites metamaterial.

However, it should also be mentioned that there are two major disadvantages of this design. First, to mitigate the wave within middle-low frequency range, soft material was chosen for the chiral honeycomb structure. This material selection compromises the mechanical strength of the structure. Second, the mass inclusion will introduce extra weight to the whole structure. Therefore, to optimize the material selections for practical applications, a more comprehensive parametric study needs to be conducted in the future.
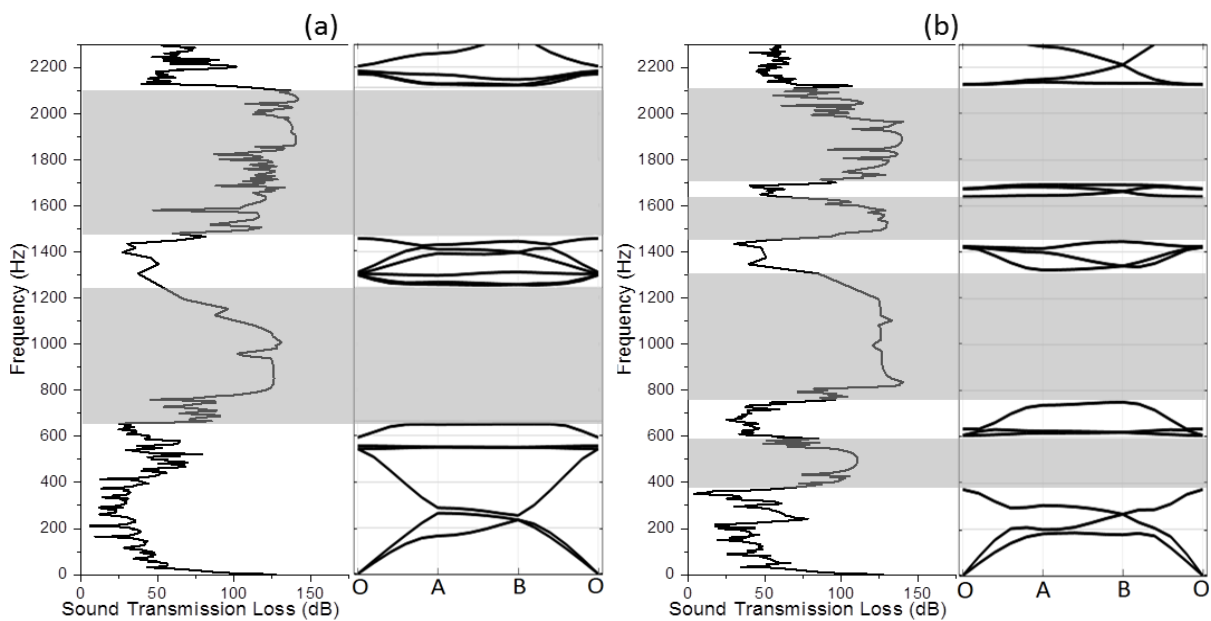

Figure 8: Sound transmission loss results of the sandwich panel with (a) reference configuration unit cell (b) modified configuration unit cell

5   CONCLUSION

In this work, a planar chiral honeycomb composite metamaterial was proposed by inserting mass inclusion into the soft hexagonal chiral honeycomb structure. Finite element analysis was adopted to investigate the dynamic characteristics of the proposed structure unit cell, as well as the sound insulation performance of the integrated sandwich panel. These two simulation results are in good agreement with each other. From the analysis and numerical studies that have been performed, it can be concluded that:

- The proposed meta-material structure is able to create multiple bandgaps for the in-plane elastic wave at middle-low frequency range (1~2300Hz).
- By properly reducing the chiral angle of the reference configuration, the vibration mode of the mass inclusion will have stronger coupling with the propagation of the wave, and two extra bandgaps induced by local resonance mechanism can be created within the target frequency range.
- The STL numerical study for integrated sandwich panel with the proposed structure unit cell shows the superior sound insulation performance within bandgaps, demonstrating the potential of the proposed structure in elastic wave mitigation application within the target frequency range.

ACKNOWLEDGEMENTS

REFERENCES

Aly, A. H., Mehaney, A., & Hanafey. 2012. 'Phononic Band Gaps in One Dimensional Mass Spring System'. In Proceedings of PIERS, 27-30. KL, Malaysia.

Brillouin, Leon. 1946. Wave Propagation in Periodic Structures: Electric Filters and Crystal Lattices. 1st ed. New York; London: McGraw-Hill book company, inc.

Ding, Y., Liu, Z., Qiu, C., & Shi, J. 2007. 'Metamaterial with simultaneously negative bulk modulus and mass-density'. Physical Review Letters, 99(9), 093904. doi:10.1103/PhysRevLett.99.093904.

Evans, Ken E. 1991. 'Auxetic Polymers: A New Range of Materials'. Endeavour 15.4: 170-4.

Griese, David, Joshua D. Summers, and Lonny Thompson. 2015. 'The effect of honeycomb core geometry on the sound transmission performance of sandwich panels'. Journal of Vibration and Acoustics 137 (2): 21011.

Huang, G. L., H. H. Huang, and C. T. Sun. 2009. 'On the negative effective mass density in acoustic metamaterials'. International Journal of Engineering Science 47 (4): 610-7.

Huang, H. H., and C. T. Sun. 2011. 'Locally resonant acoustic metamaterials with 2D anisotropic effective mass density'. Philosophical Magazine 91 (6): 981-96.

Jensen, J. S. 2003. 'Phononic band gaps and vibrations in one- and two-dimensional mass–spring structures'. Journal of Sound and Vibration, 266(5), 1053-1078. doi:10.1016/S0022-460X(02)01629-2.

Lakes, Roderic. 1987. 'Foam structures with a negative poisson's ratio'. Science 235 (4792): 1038-40.

Liu, Zhengyou, Xixiang Zhang, Yiwei Mao, Y. Y. Zhu, Zhiyu Yang, C. T. Chan, and Ping Sheng. 2000. 'Locally resonant sonic materials'. Science 289 (5485): 1734-6.

Liu, Zhengyou, C. T. Chan, and Ping Sheng. 2005. 'Analytic model of phononic crystals with local resonances'. Physical Review B 71 (1).

Liu, X. N., G. K. Hu, C. T. Sun, and G. L. Huang. 2011. 'Wave propagation characterization and design of two-dimensional elastic chiral metacomposite'. Journal of Sound and Vibration 330 (11): 2536-53.

Mead, D. M. 1996. 'Wave propagation in continuous periodic structures: Research contributions from southamton, 1964–1995'. Journal of Sound and Vibration 190 (3): 495-524.

Park, C. M., Park, J. J., Lee, S. H., Seo, Y. M., Kim, C. K., & Lee, S. H. 2011. 'Amplification of acoustic evanescent waves using metamaterial slabs'. Physical Review Letters, 107(19), 194301.

Phani, A. Srikantha, J. Woodhouse, and N. A. Fleck. 2006. 'Wave propagation in two-dimensional periodic lattices'. The Journal of the Acoustical Society of America 119 (4): 1995-2005.

Prall, D., and R. S. Lakes. 1997. 'Properties of a chiral honeycomb with a poisson's ratio of — 1'. International Journal of Mechanical Sciences 39 (3): 305,309,307,314.

Ruzzene, Massimo, Fabrizio Scarpa, and Francesco Soranna. 2003. 'Wave beaming effects in two-dimensional cellular structures'. Smart Materials and Structures 12 (3): 363-72.

Spadoni, Alessandro, Massimo Ruzzene, Stefano Gonella, and Fabrizio Scarpa. 2009. 'Phononic properties of hexagonal chiral lattices'. Wave Motion 46 (7): 435-50.

Sui, N., Yan, X., Huang, T., Xu, J., Yuan, F., & Jing, Y. 2015. 'A lightweight yet sound-proof honeycomb acoustic metamaterial'. Applied Physics Letters, 106(17), 171905. doi:10.1063/1.4919235.

Tan, K. T., H. H. Huang, and C. T. Sun. 2014. 'Blast-wave impact mitigation using negative effective mass density concept of elastic metamaterials'. International Journal of Impact Engineering 64 : 20-9.

Wang, P., Casadei, F., Shan, S., Weaver, J. C., & Bertoldi, K. 2014. 'Harnessing buckling to design tunable locally resonant acoustic metamaterials'. Physical Review Letters, 113(1), 014301.

Wu, Fugen, Zhengyou Liu, and Youyan Liu. 2002. 'Acoustic band gaps created by rotating square rods in a two dimensional lattice'. Physical Review. E, Statistical, Nonlinear, and Soft Matter Physics 66 (4 Pt 2): 046628.

Yang, Z., Mei, J., Yang, M., Chan, N. H., & Sheng, P. 2008. 'Membrane-type acoustic metamaterial with negative dynamic mass'. Physical Review Letters, 101(20), 204301. doi:10.1103/PhysRevLett.101.204301.

Zhu, R., Liu, X. N., Hu, G. K., Sun, C. T., & Huang, G. L. 2014. 'A chiral elastic metamaterial beam for broadband vibration suppression'. Journal of Sound and Vibration, 333(10), 2759. doi:10.1016/j.jsv.2014.01.009.